PREDICTION OF PERMEABILITY FROM EULER CHARACTERISTIC OF 3D IMAGES

Z. Liu[1], A. Herring[2], V. Robins[2], R. T. Armstrong[1]
[1]School of Petroleum Engineering, University of New South Wales, Kensington, New South Wales, Australia
[2]Department of Applied Mathematics, Research School of Physics and Engineering, Australian National University, Canberra, Australian Capital Territory, Australia

This paper was prepared for presentation at the International Symposium of the Society of Core Analysts held in Vienna, Austria, 27 August – 1 September 2017

ABSTRACT

The determination of absolute permeability in porous media is of great importance in hydrocarbon extraction, subsurface groundwater investigation and carbon dioxide sequestration. Permeability can be determined from empirical formulations, such as Katz-Thompson, which correlates permeability with percolation threshold. Alternatively, recent research using 2D micro-fluidic experiments and numerical simulations have demonstrated that permeability can be derived from the Euler characteristic (a topological invariant) and the number of grains, which is independent of percolation threshold. However, whether or not these new findings are applicable for three-dimensional porous media has not been verified. How to determine the number of grains also remains a question. Herein, we examine new formulations for characterizing permeability in porous media. We generate three types of stochastic models, simulate single-phase flow using Lattice Boltzmann method and calculate absolute permeability. We find that permeability in 3D pore space does not scale with the same correlation as previously published work on 2D porous media. One possible explanation to this difference is that the number of grains does not capture the resistant force in three-dimensional space. We propose a modified equation by incorporating the void ratio, which is pore volume divided by solid volume. We find that the permeability scales with the Euler characteristic, number of grains and void ratio in 3D porous media and that the scaling is unique for distinctly different stochastic models. These findings provide a new means to characterize the absolute permeability of 3D porous media from pore-scale images of distinctly different grain and pore geometries without the need of numerical simulation.

INTRODUCTION

Absolute permeability represents the ability of a porous medium to conduct fluid flow. It was first defined by Henry H. G. Darcy [1]. It is usually measured through core flooding experiment and calculated from Eq. 1, which is known as Darcy's Law.

$$K = \frac{Q\mu L}{A\Delta P} \quad (1)$$

Here K is absolute permeability, Q is flow current, μ is fluid viscosity, L is length of the core, A is cross-sectional area and ΔP, is pressure gradient. While permeability is a

simple concept there exist a wide range of different empirical relationships that link pore structure (geometry and/or topology) to permeability. These correlations are often used in the petrophysical analysis of petroleum reservoirs and/or clustering of rock properties into distinct categories.

The Carman-Kozeny equation is a well-known empirical equation where permeability is dependent on rock porosity [2], which can be seen in Eq. 2.

$$K = \frac{\phi r^2}{8\tau} \tag{2}$$

Here ϕ is rock porosity, r is effective radius and τ is tortuosity. In Figure 1, we provide the permeability versus porosity relationship for many different rock types [3]. It can be seen that there is no universal relationship between permeability and porosity, *e.g.* at 12% porosity resulting permeability value can range from 1 mD to 1D depending on the rock type. Indeed the underlying pore structure of these rocks are not the same, resulting in different effective radii and tortuosity coefficients for the same porosity. While porosity does have a strong influence in permeability, the underlying geometry and topology of the pore space are major factors that must be considered.

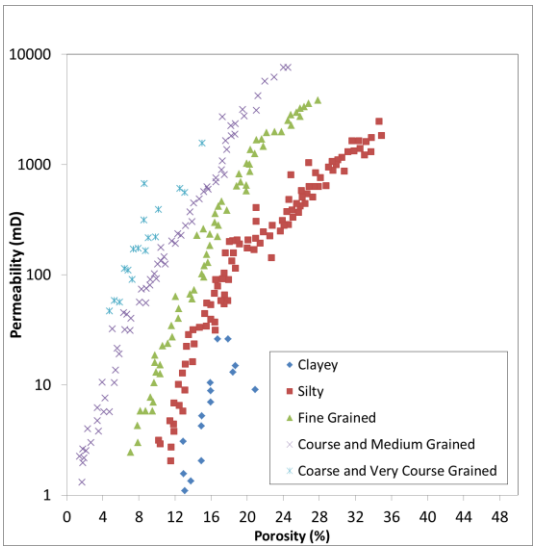

Figure 1: Modified permeability – porosity relation chart from previous work [3].

Another widely used empirical correlation is the Katz-Thompson model [4] as shown in Eq. 3.

$$K = c{l_c}^2 \left(\frac{\sigma}{\sigma_0}\right) \tag{3}$$

Here c is the constant on the order of $\frac{1}{226}$, l_c is characteristic length of the pore space, σ is conductivity of rock saturated with a brine solution of conductivity σ_0. Because electrical conductivity is influenced by the topology of the pore space this relationship implicitly captures pore topology while the geometry of the pore space is captured through the

characteristic length term (l_c). The σ/σ_0 term can be linked to porosity according to Archie's law as shown in Eq. 4.

$$\frac{\sigma}{\sigma_0} = \left(\frac{\phi-\phi_c}{1-\phi_c}\right)^{\mu} \quad (4)$$

Here ϕ_c is porosity at the percolation threshold and μ is the critical exponent. The Katz-Thompson model has been further developed by replacing the σ/σ_0 term with direct measurements of pore morphology [5]. The new formulated equation is shown is Eq. 5 and we will be referred to it as Scholz's model from hereon.

$$K = c{l_c}^2 \left(\frac{1-\chi_0}{N}\right)^{\alpha} \quad (5)$$

Here χ_0 is Euler characteristic of the conducting phase and *N* is number of grains in the granular porous media. Through topological arguments (for a 2D system), it can be shown that as $\phi \rightarrow 1$, $\frac{1-\chi_0}{N} \rightarrow 1$ and as $\phi \rightarrow 0$, $\frac{1-\chi_0}{N} \rightarrow 0$. Therefore $\frac{1-\chi_0}{N}$ is analogous to (σ/σ_0) from Katz-Thompson because as $\phi \rightarrow 1$, $(\sigma/\sigma_0) \rightarrow 1$ and as $\phi \rightarrow 0$, $(\sigma/\sigma_0) \rightarrow 0$. In order to apply Scholz's model to 3D systems, the Euler characteristic of the pore space can be measured from segmented X-ray microtomography (micro-CT) images. However, calculating the number of grains (*N*) in the context of real reservoir rock is not straightforward. In Scholz *et al.* [5], the number of grains (*N*) was an input parameter from their stochastically generated models and each grain had constant volume, which is not realistic for geologic materials. For the practical application of Scholz's model, *N* must be directly measured from micro-CT images and it must accommodate different grain sizes.

Regardless of the practical problems associated with Scholz's model, the results are intriguing because they demonstrate a universal permeability relationship for stochastically generated 2D porous media. The tested porous media displayed different scaling relationships for ${cl_c}^2$ versus ϕ; however, once ${cl_c}^2$ versus $\frac{1-\chi_0}{N}$ was considered the data collapsed onto a single relationship. The main drawback of this study was that only 2D systems were considered and the proposed relationship has yet to be applied to real rock data. The results however warrant further studies and suggest that Scholz's model could provide a universal relationship between permeability and pore topology.

A key parameter in Scholz's model is the 2D Euler characteristic, which is a topological invariant that describes the connectivity of a binary object. The Euler characteristic has been previously used to characterize pore morphology of soils and reservoir rocks [6], two-phase flow and relative permeability [7-10], and non-wetting phase trapping for application to CO_2 sequestration [11]. The Euler characteristic can be determined from segmented pore scale images of reservoir rocks. The most intuitive way to think about the Euler characteristic is in terms of its Betti numbers (β_i).

$$\chi = \beta_0 - \beta_1 + \beta_2 \quad (5)$$

For a 3D object, β_0 is the number of components, β_1 is the number of inequivalent loops and β_2 is the number of cavities (enclosed voids). Take a donut as an example, shown in Figure 2, where the number of components is 1 (β_0=1) and number of inequivalent loops is 1 (β_1=1) since we are considering a solid donut. In describing the topology of the pore space of a porous rock, it can be assumed that the solid matrix is connected, so that $\beta_2 = 0$. In this case, the Euler number reduces to the difference between the number of discrete components and inequivalent loops. If all pore space is connected via one pathway or another, and there are no isolated pore spaces, then $\beta_0 = 1$. As the number of loops decreases the Euler number becomes less negative and will eventually become positive, at which point the system will no longer percolate [12].

Figure 2: A solid donut with a β_0 of 1, β_1 of 1 and β_2 of 0.

Recent developments in digital rock technologies have given us access to detailed information on pore space morphology using micro-CT imaging [13, 14]. One method to calculate permeability from micro-CT images is pore network modelling [15]. In addition to the pore network modelling approach, direct numerical simulations on porous media images have been developed, including finite difference methods [16] and Lattice-Boltzmann methods (LBM) [17], and these achieve reasonable predictions of permeability compared with experiments. The Lattice-Boltzmann method has been shown to be a valid approach in predicting absolute permeability for sandstone with limited resolution [18]. However, we would like to develop a simple approach for estimating reservoir rock permeability by measuring pore morphology.

Herein, we verify Scholz's model by simulating single-phase flow through quasi-two-dimensional (q2D) geometries and 3D systems. For the 2D models, we explore different ways to determine *N* and then extend our studies to 3D systems with different grain sizes. Recent developments in digital rock technology have given us access to detailed information on pore space morphology using micro-CT imaging [13, 14] and Scholz's model provides a novel approach to utilize this information. We attempt to apply Scholz's model to more realistic pore morphologies and thus attempt to provide a simple/convenient methodology to predict the absolute permeability of digital images. This approach could also provide a robust way to characterize rock types that have distinguishably different pore morphologies by providing a universal relationship between permeability and pore morphology.

MODEL GENERATION

We generate quasi-two-dimensional and 3D models for testing and extending Scholz's model. The quasi-two-dimensional (q2D) models generated are similar to Scholz's work including round models (RM) and ellipse models (EM) in a 4000x4000x10 domain size. The round models have a radius of 30 voxels. The ellipse models have a constant aspect ratio $a/b = 8$, where a is the long semi-axis and b is the short semi-axis of the ellipse. Additionally, we add square models (SM) as a new validation model to our work. The three types of q2D models are shown in Figure 3. For all of these models the number of grains (N) is an input parameter and each grain is added to a random location. For the ellipse model, each ellipse also has a random orientation. We control the number of elements (round, ellipse, square) to generate models with a range of different porosities.

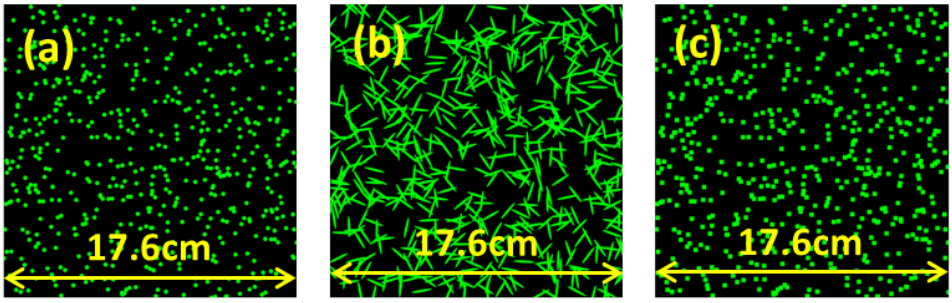

Figure 3: Generated 2D models with 600 Grains, (a) Round Model (b) Ellipse Model and (c) Square Model.

We also test three distinct 3D models as shown in Figure 4: (a) Sphere Model (480x480x480 domain): generated by randomly placing spheres with random radii following a Gaussian distribution (average radius is 20 voxels, standard deviation is 4 voxels) within the domain. The number of grains (N) added controls the porosity; (b) Stick Model (480x480x480 domain): generated by randomly placing sticks with random orientation within the domain. The length-width-height ratio is 2:2:15. The number of grains (N) added controls the porosity; (c) Robuglass Model (1000x1000x572 domain): a synthetic porous media is imaged with micro-CT [19, 20] and then derivative models are generated by running either erosion or dilation filters on the segmented image to reduce/increase the porosity. The number of grains (N) must be measured.

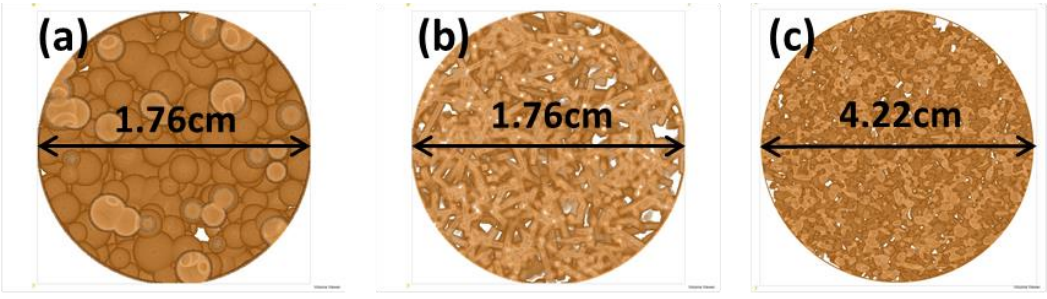

Figure 4 Generated 3D Models with 600 Grains, (a) random sphere model with 600 grains (b) random stick model with 9000 grains and (c) Robuglass model with erosion of 4 voxels.

CRITICAL PORE DIAMETER

For the q2D structures considered here, the critical pore diameter can be limited by the system height h. When the q2D critical pore diameter is larger than the height h, the limiting hydrodynamic length is determined by, h, i.e., $l_c = min(D_c, h)$.

The q2D and 3D critical diameter D_c is calculated from the Euclidean Distance Map (EDM). By thresholding the EDM with different radii r, a percolation test is performed to check if the system can percolate or not, the critical diameter D_c is two times the radius between percolation and non-percolation at the onset of percolation.

GRAIN NUMBER DETERMINATION

Input Grain Number

The input grain number N_i is available in q2D models, 3D Sphere Model and 3D Stick Model as an input. For 3D Robuglass Models, N_i is not available and the grain number must be determined using other methods. We must determine how to measure *N* if there is to be any practical application of Scholz's model applied to digital rock images. Herein we test two different approaches for measuring *N*.

Weighted Grain Number

The weighted grain number N_w is the grain number determined by Eq. 6.

$$N_w = \frac{V_{gtot}}{V_{element}} \tag{6}$$

Here V_{gtot} is the total volume of grains and $V_{element}$ is the volume of a single grain, or the mean grain volume as determined from pore-scale images. N_w is directly available in q2D models, 3D Sphere Model and Stick Model and can be measured from all other models by estimating mean grain size after running a grain separation algorithm (watershed) on the segmented images.

Persistence Grain Number

The persistence grain number N_p is calculated from the persistent homology signatures of the data as measured using the software package Diamorse [21]. In the persistent homology analysis, a signed Euclidian distance transform (SEDT) is calculated from the segmented image data; this identifies local minima at the center of pore bodies within the pore space of the system and local maxima at the center of solid grains. A level-set growth process is carried out on this Euclidean distance transform: topological features β_0, β_1 and β_2 are measured for the data set at each level-set distance value; as the level-set value increases from local minima (pore bodies) to local maxima (grain interiors) topological features are tracked, and their "persistence" (the difference in distance values for which individual β features appear and vanish) is measured. For our analysis, a feature whose persistence is less than one unit in the voxel size is considered to be insignificant and merged with an adjacent feature. From this persistent homology

perspective, cavities (β_2 features) will appear in the SEDT as the level-set threshold value increases beyond the grain-pore space interface and local maxima (grains) become separated; the total number of β_2 features that have a persistence greater than one unit of distance provides an estimate for the number of topologically-relevant grains in the sample.

EULER CHARACTERISTIC

Before the Euler characteristic is calculated, a spanning cluster is extracted with a 6-connectivity check, so that dead pores, i.e. pores inside the grains, contribute neither to the total porosity nor the Euler characteristic. Euler characteristic and the Betti numbers are determined using pore-scale image processing software Mango [22].

LATTICE-BOLTZMANN SIMULATION OF SINGLE PHASE FLOW

The Lattice-Boltzmann model used here is the D3Q19 (3D lattice with 19 possible momenta components) in the Morphy software package [18, 23]. The single relaxation time (SRT) Bhatnager–Gross–Krook (BGK) model is used as the collision model. The boundary condition of the inlet and outlet is periodic boundary condition and fluid-solid boundary condition is bounce-back boundary condition. All of the simulations are performed on the Raijin supercomputer from National Computational Infrastructure (NCI). The average velocity is calculated from the velocity field and then used to determine permeability using Eq. 1.

2D VERIFICATION OF SCHOLZ'S MODEL

Figure 5a shows the numerically determined permeability (normalized by $cl_c{}^2$) versus the $(\phi - \phi_c)/(1 - \phi_c)$ according to Eq. 3 and Eq. 4. We can see that each q2D model follows a different trend when only porosity is considered. We also tested Scholz's model and found a relationship between $K/(cl_c{}^2)$ and $(1 - \chi)/N_i$ that is similar to what is reported by Scholz *et al.* [5]. In Figure 5b, we can see that each q2D model collapses to a single relationship when the topology of the pore space is considered.

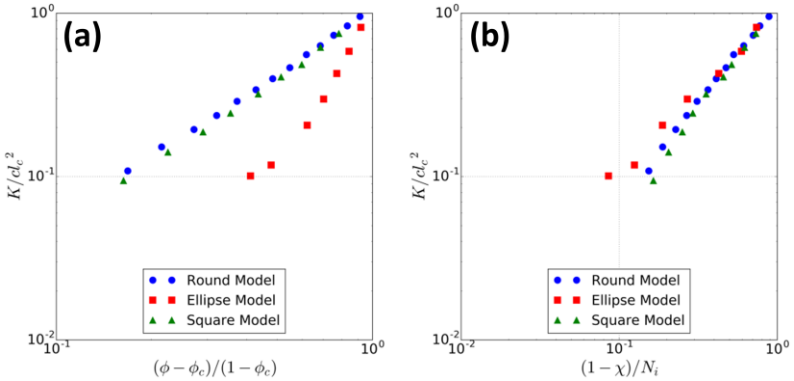

Figure 5: (a) $K/cl_c{}^2$ versus $(\phi - \phi_c)/(1 - \phi_c)$ for q2D models (b) $K/cl_c{}^2$versus $(1 - \chi)/N_i$ for q2D models using Scholz's model

However, for the data presented in Figure 5b, N is an input parameter. For the practical application of this work, we need to measure N from the pore scale images. For this we test the weighted grain number (N_w) and persistent grain number approaches (N_p). In Figure 6 we show how the persistence model is able to partition the grains for the q2D models. It can be seen that for the spherical and square shaped grains the persistent homology approach appears to capture each grain element whereas for the ellipse grains when multiple ellipses overlap then additional grains are measured. Furthermore in Figure 7, we compare the input grain number (N_i) to the measured grain numbers for all three of the q2D models. We find that for the Ellipse Model, the best match in comparison to N_i is with $N_w$whereas N_p overestimates the number of grains. It appears that the persistent homology of the SEDT does not accurately identify overlapping grains with irregular oblong shapes. For the round and square models, both N_w and N_p produce lower grain number estimates than N_i at high grain density; the reason behind this is that in model generation the generated grains can overlap with each other but the grain number still adds to N_i. In all three cases, at low grain density the N_w and N_p are able to measure a grain number near N_i. However, as added grains start to overlap, the measured values depart from N_i.

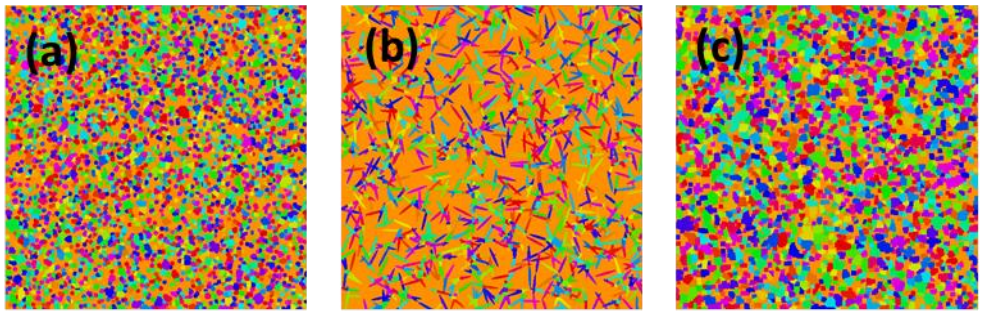

Figure 6: Grain partition diagrams for (a) Round Model (b) Ellipse Model and (c) Square Model from persistence homology. Orange represents pore space and other colors are used to label individual grains.

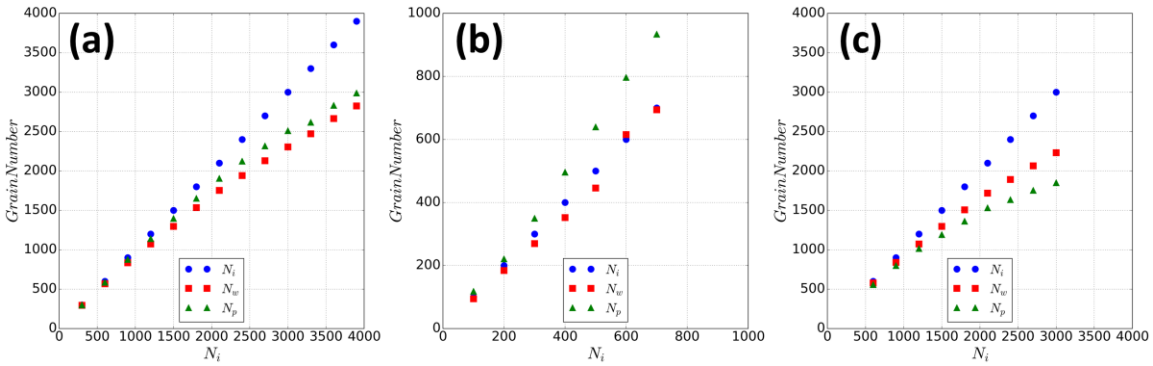

Figure 7: Grain number (input grain number, N_i; weighted grain number, Nw, and persistence grain number Np) versus input grain number for (a) Round Model (b) Ellipse Model and (c) Square Model.

The implication of these results is seen in Figure 8 where the universal relationship presented in Figure 5b (using N_i) no longer holds. At low grain density, we are able to measure a grain number that is consistent with N_i and thus the data collapses to a single relationship. However, as grain density increases, the datasets follow different relationships because the difference between the measured and input grain numbers starts to deviate. While this might not be an issue in real rock samples, because grains do not overlap as in our stochastically generated models, this could be an issue in rock types with irregular or oblong shaped grains.

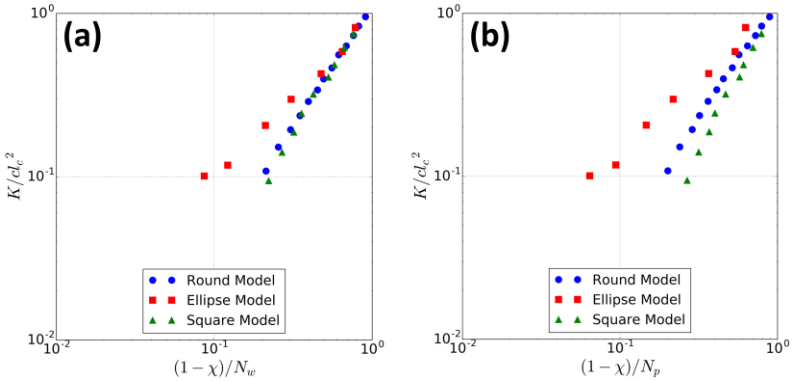

Figure 8: (a) $K/cl_c^{\,2}$ versus $(1-\chi)/N_w$ for q2D models (b) $K/cl_c^{\,2}$versus $(1-\chi)/N_p$ for q2D models.

3D EXTENSION OF SCHOLZ'S MODEL

First we plot $K/(cl_c^{\,2})$ versus $(\phi-\phi_c)/(1-\phi_c)$ in Figure 9a. It can be seen that each dataset follows a slightly different scaling relationship. We also plot $K/(cl_c^{\,2})$ versus β_1/N_p in Figure 9b according to Scholz's model. We use β_1 instead of $(1-\chi)$ because in 3D the Euler characteristic is dominated by β_1, which best represents the connectivity, and we use N_p as the number of grains. Scholz's model does not seem to predict a single trend relationship between $K/(cl_c^{\,2})$ and β_1/N_p. The reason for this can be explained in Figure 10. Intuitively, and as described in the introduction, as $\phi\rightarrow 1$, $\frac{K}{(cl_c^{\,2})} \rightarrow 1$, and as $\phi\rightarrow 0$, $\frac{K}{(cl_c^{\,2})} \rightarrow$ 0-; thus, the same limits will apply to any topological metrics describing permeability. We observe that these limits apply for $(1-\chi)/N_p$ in 2D, however, this does not occur for $\frac{\beta_1}{N_p}$ in 3D.

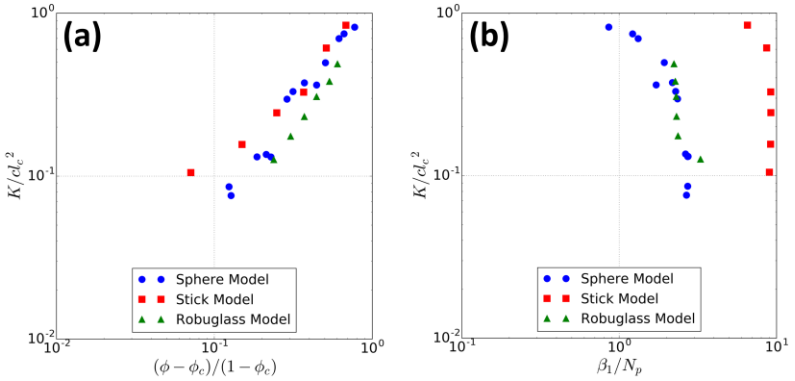

Figure 9: (a) $K/cl_c^{\,2}$ versus $(\phi-\phi_c)/(1-\phi_c)$ for 3D models (b) $K/cl_c^{\,2}$ versus β_1/N_p.

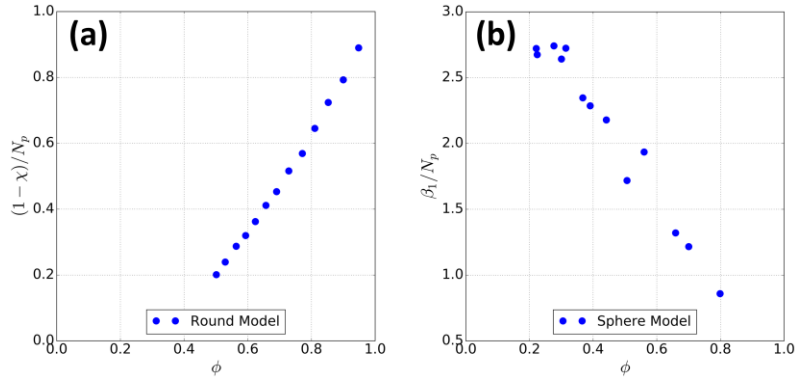

Figure 10: Euler characteristic versus porosity, (a) 2D Round Model (b) 3D Sphere Model.

Noting that the variable N_p perhaps does not fully describe the resistance to flow in 3D, we incorporate the void ratio e, which is equal to $\phi/(1-\phi)$. When we plot $\beta_1/N_p \times e$ versus porosity, we can generate a trend similar to that observed for the 2D systems, compare Figures 10a and 11a. We plot $K/(cl_c^{\,2})$ versus β1/Np*e in Figure 11b and find that all 3 datasets provide very similar scaling relationships, i.e. the slope of each line is similar. The curves could be collapsed to a single relationship by adjusting the constant parameter c; however, at this time we cannot justify the physical significance of this.

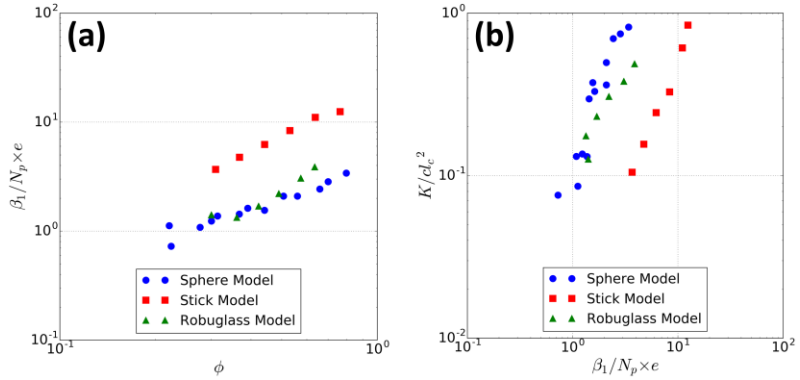

Figure 11: (a) $\beta_1/N_p \times e$ versus ϕ for 3D models (b) $K/cl_c^{\,2}$ versus $\beta_1/N_p \times e$ for 3D models

CONCLUSION

We verify Scholz's model by simulating single-phase flow in generated q2D models. With regards to the grain number, we implement distinct methods to measure grain count and show that these methods compare well to the input parameter from stochastically generated media when the number of overlapping grains is low. We then extend Scholz's model by simulating single-phase flow in 3D porous media, and we find that by adding a new parameter, the void ratio, the modified Scholz's equation is able to provide a similar scaling exponent for all of the tested models.

ACKNOWLEDGEMENTS

This research was undertaken with the assistance from resources provided at the NCI National Facility systems through the National Computational Merit Allocation Scheme and the Australian Government provided funding through an Australian Research Council (ARC) Discovery Project (DP160104995).

REFERENCES

1. H. Darcy, *Les fontaines publiques de la ville de Dijon: exposition et application*, Victor Dalmont, (1856).
2. P.C. Carman, *Flow of gases through porous media*, Academic press, (1956).
3. D. Tiab and E. Donaldson, "Petrophysics, Theory and practice of measuring reservoir rock and fluid transport properties, Gulf Publ," *Co., Houston, Texas*, (1996), 205-220.
4. A. Katz and A. Thompson, "Quantitative prediction of permeability in porous rock," *Physical review B*, (1986) **34**, 11, 8179.
5. C. Scholz, F. Wirner, J. Götz, U. Rüde, G.E. Schröder-Turk, K. Mecke and C. Bechinger, "Permeability of porous materials determined from the Euler characteristic," *Physical review letters*, (2012) **109**, 26, 264504.
6. H.-J. Vogel, U. Weller and S. Schlüter, "Quantification of soil structure based on Minkowski functions," *Computers & Geosciences*, (2010) **36**, 10, 1236-1245.
7. Z. Liu, A. Herring, C. Arns, S. Berg and R.T. Armstrong, "Pore-Scale Characterization of Two-Phase Flow Using Integral Geometry," *Transport in Porous Media*, (2017) **118**, 1, 99-117.
8. R.T. Armstrong, J. McClure, M. Berill, M. Rücker, S. Schlüter and S. Berg, "Flow regimes during immiscible displacement," *Petrophysics*, (2017) **58**, 01, 10-18.
9. R.T. Armstrong, J.E. McClure, M.A. Berrill, M. Rücker, S. Schlüter and S. Berg, "Beyond Darcy's law: The role of phase topology and ganglion dynamics for two-fluid flow," *Physical Review E*, (2016) **94**, 4, 043113.
10. S. Schlüter, S. Berg, M. Rücker, R. Armstrong, H.J. Vogel, R. Hilfer and D. Wildenschild, "Pore-scale displacement mechanisms as a source of hysteresis for two-phase flow in porous media," *Water Resources Research*, (2016).

11. A.L. Herring, E.J. Harper, L. Andersson, A. Sheppard, B.K. Bay and D. Wildenschild, "Effect of fluid topology on residual nonwetting phase trapping: Implications for geologic CO2 sequestration," *Advances in Water Resources*, (2013) **62, Part A**, 47-58.
12. H.-J. Vogel, *Topological Characterization of Porous Media*, in *Morphology of Condensed Matter*, K. Mecke and D. Stoyan, Editors. 2002, Springer Berlin Heidelberg. p. 75-92.
13. D. Wildenschild and A.P. Sheppard, "X-ray imaging and analysis techniques for quantifying pore-scale structure and processes in subsurface porous medium systems," *Advances in Water Resources*, (2012) **51**, January 2013, 217–246.
14. S. Berg, H. Ott, S.A. Klapp, A. Schwing, R. Neiteler, N. Brussee, A. Makurat, L. Leu, F. Enzmann, J.O. Schwarz, M. Kersten, S. Irvine and M. Stampanoni, "Real-time 3D imaging of Haines jumps in porous media flow," *Proceedings of the National Academy of Sciences of the United States of America*, (2013) **110**, 10, 3755-3759.
15. H. Dong and M.J. Blunt, "Pore-network extraction from micro-computerized-tomography images," *Physical review E*, (2009) **80**, 3, 036307.
16. P. Mostaghimi, M.J. Blunt and B. Bijeljic, "Computations of absolute permeability on micro-CT images," *Mathematical Geosciences*, (2013) **45**, 1, 103-125.
17. S. Chen and G.D. Doolen, "Lattice Boltzmann method for fluid flows," *Annual review of fluid mechanics*, (1998) **30**, 1, 329-364.
18. C.H. Arns, M.A. Knackstedt and N.S. Martys, "Cross-property correlations and permeability estimation in sandstone," *Physical Review E*, (2005) **72**, 4, 046304.
19. S. Berg, M. Rücker, H. Ott, A. Georgiadis, H. van der Linde, F. Enzmann, M. Kersten, R. Armstrong, S. de With and J. Becker, "Connected pathway relative permeability from pore-scale imaging of imbibition," *Advances in Water Resources*, (2016) **90**, 24-35.
20. M. Rücker, S. Berg, R. Armstrong, A. Georgiadis, H. Ott, A. Schwing, R. Neiteler, N. Brussee, A. Makurat and L. Leu, "From connected pathway flow to ganglion dynamics," *Geophysical Research Letters*, (2015).
21. O. Delgado-Friedrichs, V. Robins and A. Sheppard, "Skeletonization and partitioning of digital images using discrete morse theory," *IEEE transactions on pattern analysis and machine intelligence*, (2015) **37**, 3, 654-666.
22. A. Sakellariou, C.H. Arns, A.P. Sheppard, R.M. Sok, H. Averdunk, A. Limaye, A.C. Jones, T.J. Senden and M.A. Knackstedt, "Developing a virtual materials laboratory," *Materials Today*, (2007) **10**, 12, 44-51.
23. C. Arns, F. Bauget, A. Sakellariou, T. Senden, A. Sheppard, R. Sok, A. Ghous, W. Pinczewski, M. Knackstedt and J. Kelly, "Digital core laboratory: Petrophysical analysis from 3D imaging of reservoir core fragments," *Petrophysics*, (2005) **46**, 04.